Deep-Sea Research, Vol. 27A, pp. 693 to 714

0198-0149/80/0901-0693 $02.00/0

Surface conditions in the eastern equatorial Pacific related to the intertropical convergence zone of the winds

J. R. DONGUY* and C. HENIN*

(*Received* 17 *August* 1979; *accepted* 3 *January* 1980; *final revision received* 1 *February* 1980)

Abstract—Surface temperature and salinity data gathered by merchant ships along the Tahiti–Panama track from 1955 to 1978 are considered in relation to cloud cover. Equatorial upwelling is associated with strong cloudiness at its northern boundary. The cloudiness indicates the presence of the intertropical convergence zone of the winds. During the seasonal absence of upwelling, the position of the intertropical convergence zone is southernmost and the cloudy zone is south of the equator. In the case of El Niño, equatorial upwelling weakens, the northern cloud cover is minimal, and the intertropical convergence zone may shift southward. During El Niño, the surface salinity is affected by the position of the intertropical convergence zone.

INTRODUCTION

THERE ARE few meteorological and oceanographical data from the eastern equatorial Pacific. However, in addition to the 1967–68 period during which Eastropac cruises gave a good description of the area, historical data from ship's logs are available from 1955 to 1973; a surface observation system, operated by the Centre ORSTOM de Noumea, was started in 1970 with the help of French naval vessels and merchant ships. The following data will be used:

(1) Historical data issued by the French "Meteorologie Nationale" and gathered by merchant ships between Tahiti (17°33'S, 149°37'W) and Panama (8°57'N, 79°33'W). The data start in 1955 and run through the end of 1973; there are about 40,000 observations of sea surface temperature and routine meteorological observations.

(2) Surface data from merchant ships systematically gathered between Tahiti and Panama by the Centre ORSTOM de Noumea starting in October 1974. They include meteorological data, surface temperature, and salinity. Unfortunately, no data are available from December 1973 to October 1974.

(3) Surface data (meteorological observations, temperature, and salinity) gathered since 1970 in the eastern Pacific by French naval vessels and merchant ships. The data are adequate, along with other data from data banks, to draw up quarterly charts for each year between 1970 and 1977.

Before 1974, sea surface temperatures were usually read to 0.5°C on thermometers in engine intakes at an approximate depth of 5 m. Seawater samples gathered simultaneously were kept in sealed bottles with salinities determined later with an inductive salinometer. Since 1974, surface temperatures and salinities have been obtained from bucket samples.

* Centre ORSTOM de Noumea, B.P. A5, Noumea, Nouvelle-Caledonie, France.

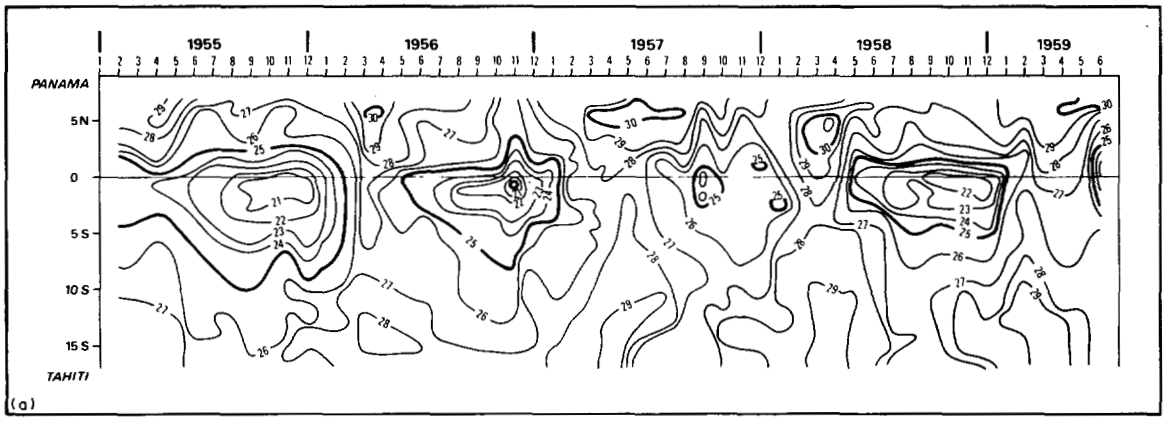
1955
1956
1957
1958
1959
PANAMA
5N
0
5S
10S
15S
TAHITI
(a)

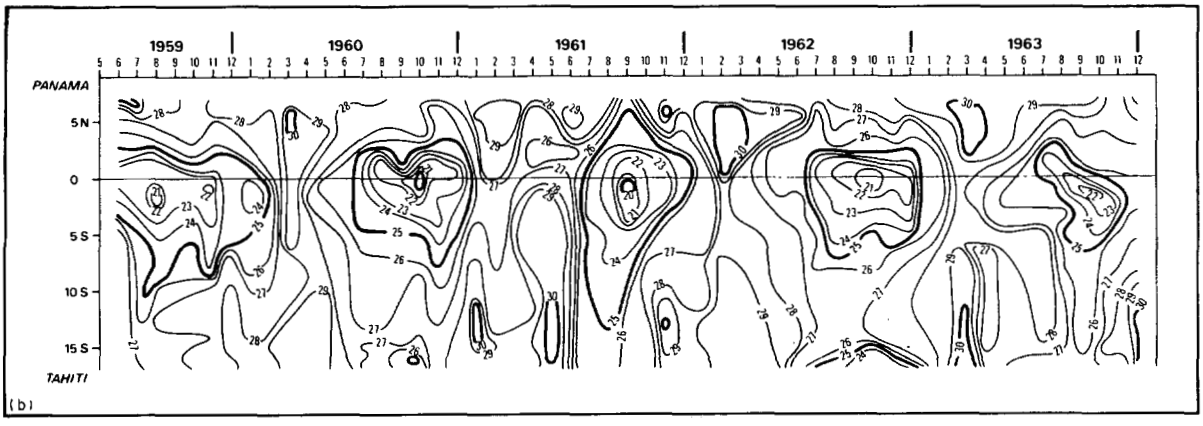
1959
1960
1961
1962
1963
PANAMA
5N
0
5S
10S
15S
TAHITI
(b)

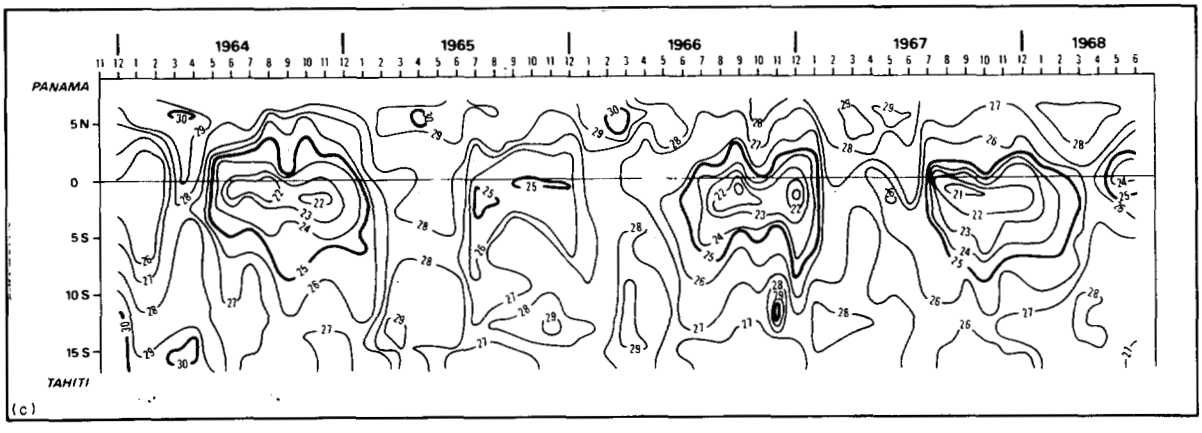
1964
1965
1966
1967
1968
PANAMA
5N
0
5S
10S
15S
TAHITI
(c)

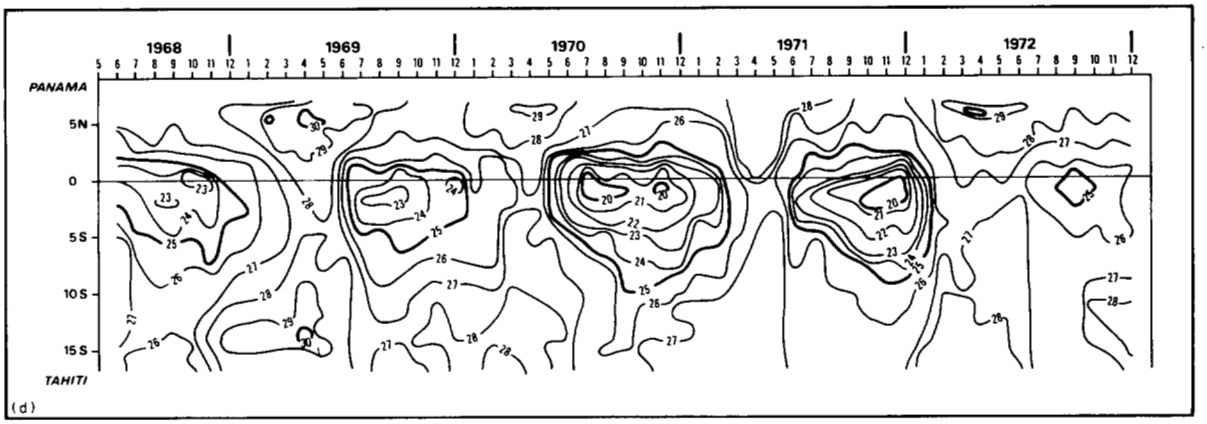

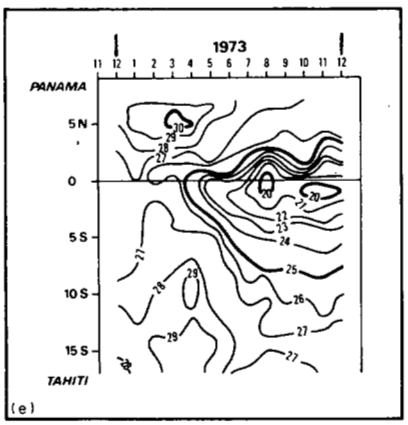

Fig. 1. Surface temperature, in degree Celsius, along the track between Tahiti and Panama, 1955–1978.

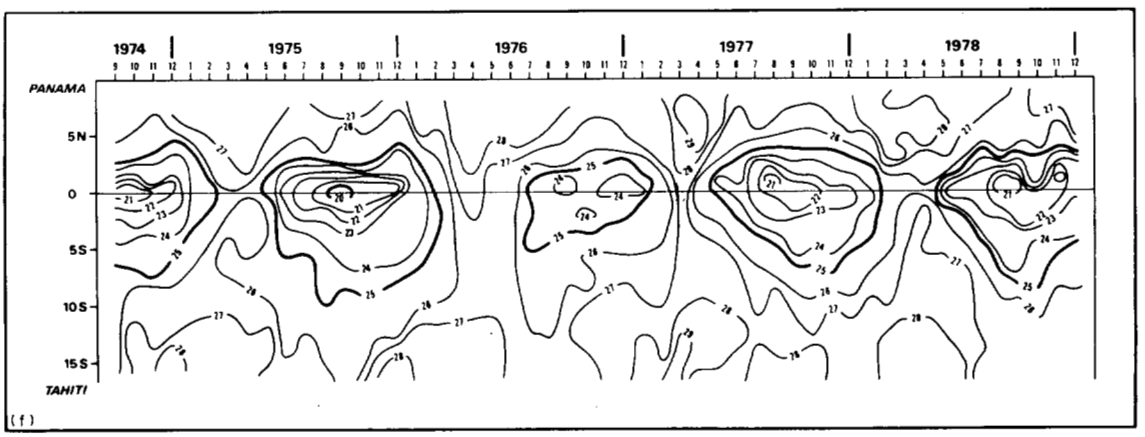

Before 1974, one observation was made every 6 h, i.e., about every 90 nautical miles, but after 1974 only one about every 120 nautical miles. Before 1965 there was one voyage per month, but since then at least two have been available each month after 1965. For each time series, the data have been averaged by latitude and by month and plotted on space–time diagrams.

Surface temperature in the eastern Pacific

1. *Seasonal variations.* A space–time diagram showing the 1955–1978 surface temperatures from Tahiti to Panama is shown in Fig. 1. The diagram emphasizes distinct seasonal variations. From January to June the surface water is warm; from July to December it is cold. A standard year has been drawn from the 1955–1973 temperatures (Fig. 2). From July to December, south of 10°S, the cold water is due to the southern winter. On the equator the cold water is due to the equatorial upwelling. From September to November the surface water is usually colder than 22°C between the equator and 2°S and in some years colder than 20°C (1956, 1960, 1961, 1970, 1971, 1973, 1975). From January to June, warm water south of 10°S is due to the southern summer and close to the equator it is due to the absence of equatorial upwelling; however, the temperature maximum at 5°N, also shown by the Eastropac Atlases in February–March 1967 and 1968 (LOVE, 1972, 1975), is difficult to explain. The conditions along the Tahiti–Panama track may be compared with those along the Samoa–Hawaii track (HIRES and MONTGOMERY, 1972). Due to the distance between the tracks (6000 km), the equatorial and the northern conditions are almost opposite: at 160°W the coldest upwelled water occurs in February, at

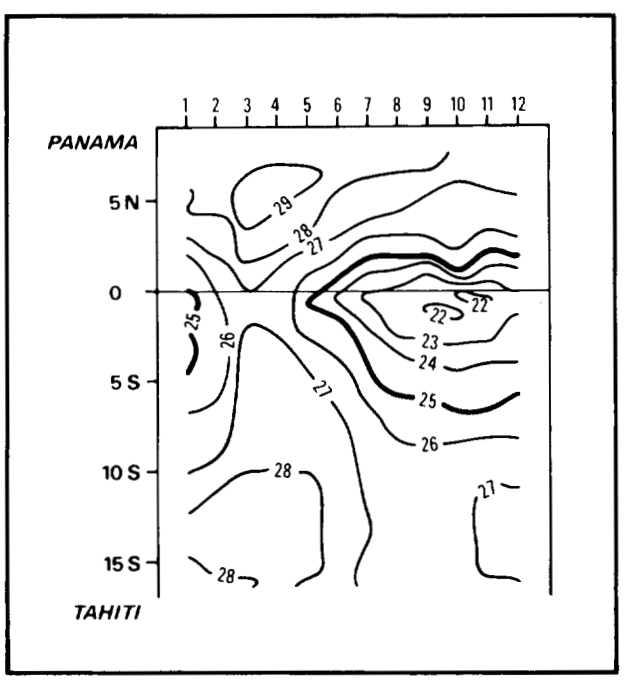

Fig. 2. Mean surface temperature, in degree Celsius, along the track between Tahiti and Panama.

100°W in October; at 160°W the warmest water occurs at 5°N in October, at 100°W in April; however, the influence of the south warm season occurs at the same time (March–June).

The space–time diagram describing the speed and direction of the wind (Fig. 3) according to ATKINSON and SADLER (1970) shows that on the equator from June to November the wind has an easterly component and a speed between 10 and 15 knots (1 knot = 1.853 km h^{-1}). From December to May it also has an easterly component but a speed of less than 10 knots. Thus, the equatorial upwelling is probably induced by easterly winds whose speed is the determining cause, the shift of the cold water towards the south being explained by advection from the South American coast and also by the influence of the southerly component of the wind (CROMWELL, 1953). On Fig. 3 the convergence zone of the winds is shown by the area north of 5°N with a speed less than 5 knots.

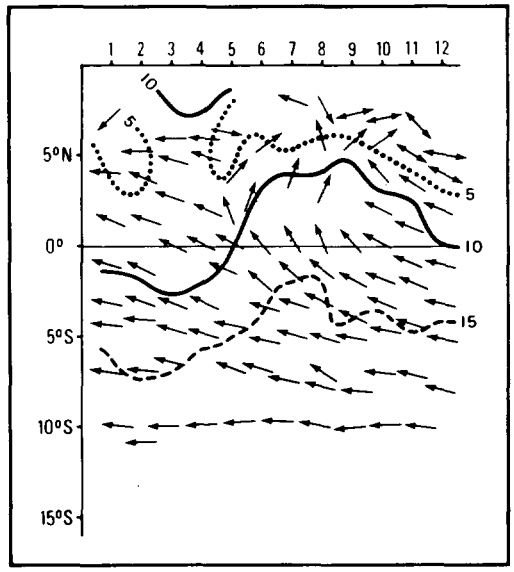

Fig. 3. Mean speed and direction of the wind, along the track between Tahiti and Panama. The speed is indicated in knots and the direction is marked by arrows.

The 1955–1973 series on cloud cover in oktas as observed by the ships is represented on a space–time diagram (Fig. 4). The series and the average of the data are shown in the same kind of diagram (Fig. 5), in which distinct seasonal variations are apparent. North of the equator, extensive cloud cover (more than 6 oktas) occurs from May to February with a maximum (7 oktas) from July to November when the influence reaches 3°S latitude. From 7°N to 3°S between February and May the cloud cover is less, with a minimum at the equator (less than 4 oktas). In the southern hemisphere, maximum cloud cover (more than 4 oktas) occurs from January to May between 2 and 6°S. All these features agree with the charts of ATKINSON and SADLER (1970).

It is possible to compare the observations with the 1965–1973 series of cloud cover observations from satellites along the same track (SADLER, UDA and KILONSKY, 1976) (Fig. 6). The general features are the same: extensive cloud cover north of the equator with

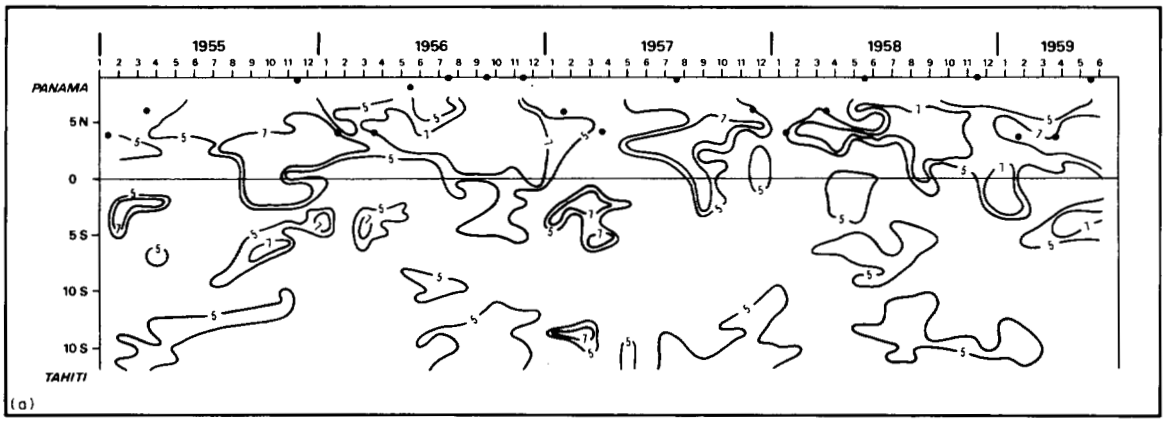
1955
1956
1957
1958
1959
PANAMA
5 N
0
5 S
10 S
10 S
TAHITI
(a)

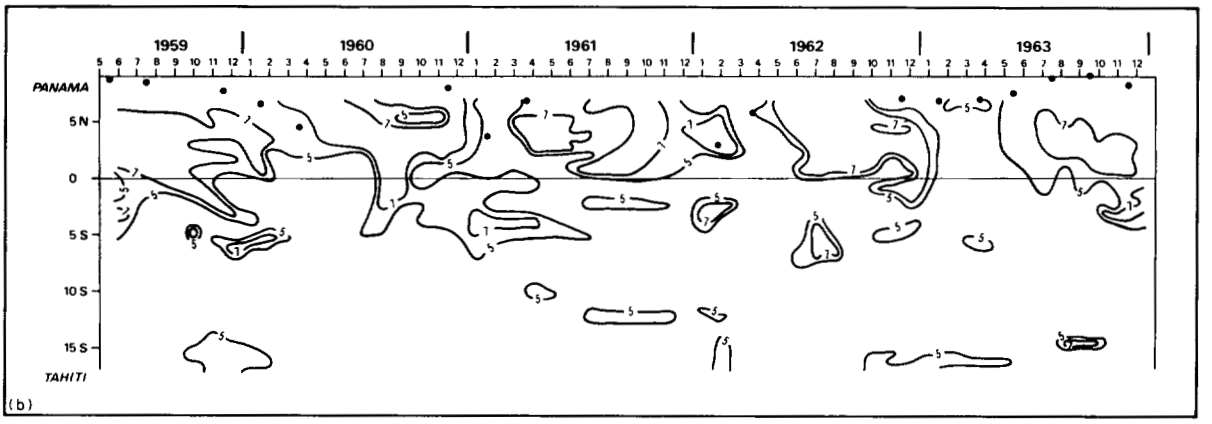
1959
1960
1961
1962
1963
PANAMA
5 N
0
5 S
10 S
15 S
TAHITI
(b)

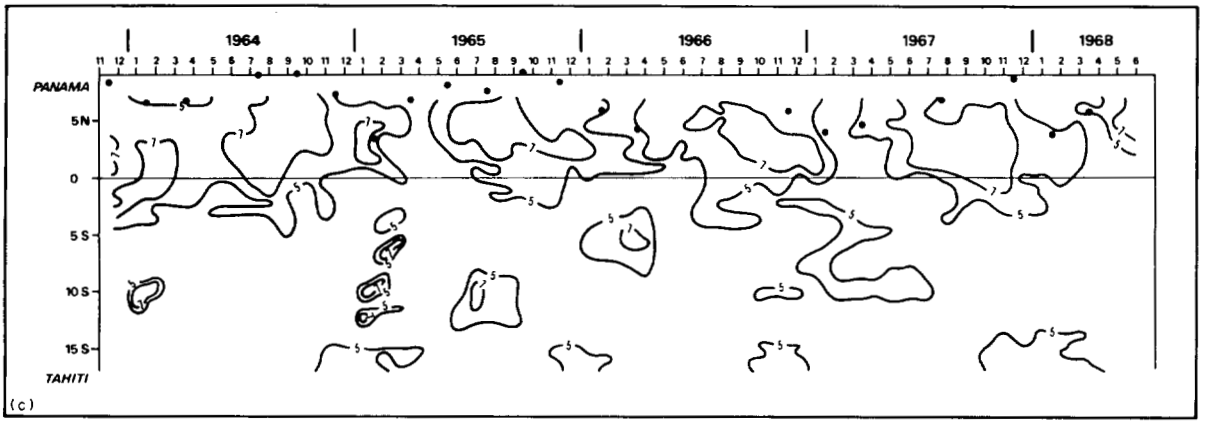
1964
1965
1966
1967
1968
PANAMA
5N
0
5 S
10 S
15 S
TAHITI
(c)

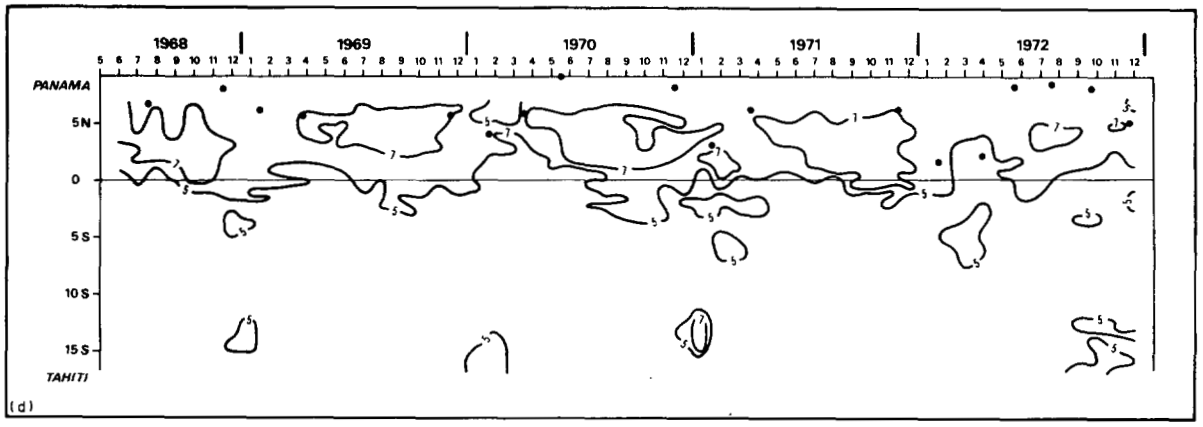

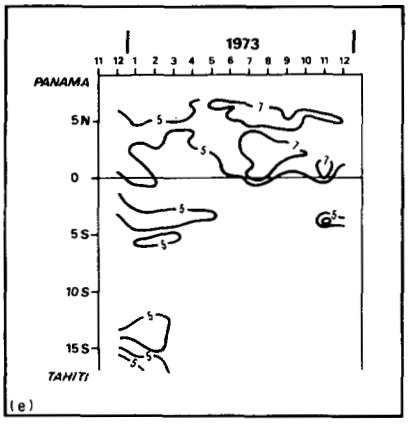

Fig. 4. Cloud cover observed by ships, in oktas, along the track between Tahiti and Panama, 1955–1973. The bimonthly position of the intertropical convergence zone of the winds is marked by a point.

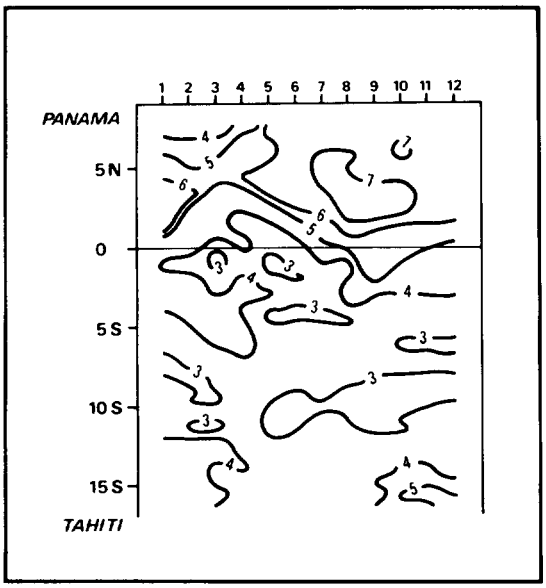

Fig. 5. Mean cloud cover, in oktas, along the track between Tahiti and Panama.

a maximum from June to November, less cloud cover south of the equator with, however, a maximum from February to May. On the other hand, the values differ: for example, the maximum cloud cover observed from satellites is 5 to 6 oktas north of the equator instead of the 7 oktas observed from ships.

In summary, from comparing the mean sea surface temperature (Fig. 2), the speed and direction of the wind (Fig. 3), and the cloud cover (Fig. 5), the following features are evident:

(1) From June to December equatorial upwelling is induced by southeast winds with a speed of more than 10 knots. The upwelling is associated with cloud covers of more than 4 oktas.

(2) From January to May the weakness of the east wind results in the cessation of equatorial upwelling. At this time the cloud over the equator is less than 4 oktas but from 2 to 5°S it is more than 4 oktas.

Equatorial upwelling is usually associated with extensive cloud cover at its northern boundary. The position of the intertropical convergence zone of the winds (Fig. 4), estimated from WYRTKI and MEYERS (1975) by considering the minimum of the wind speed and the convergence of the streamlines, is always north of the cloud zone. It also appears that on the equator the sea surface temperature maximum usually occurs between February and May, when equatorial upwelling subsides because of the wind speed minimum. The temperature maximum coincides with an equatorial cloud cover minimum (Fig. 5), in accordance with the cloud-coverage charts from ATKINSON and SADLER (1970). The feature is in contradiction with the BJERKNES (1966, 1969) hypothesis that high sea-surface temperature enhances convection and increases cloudiness. However, RAMAGE (1977), after studying hydroclimatic conditions at Canton Island (2°49'S, 171°43'W) during the 1972–1973 El Niño period, also disagreed with the BJERKNES hypothesis.

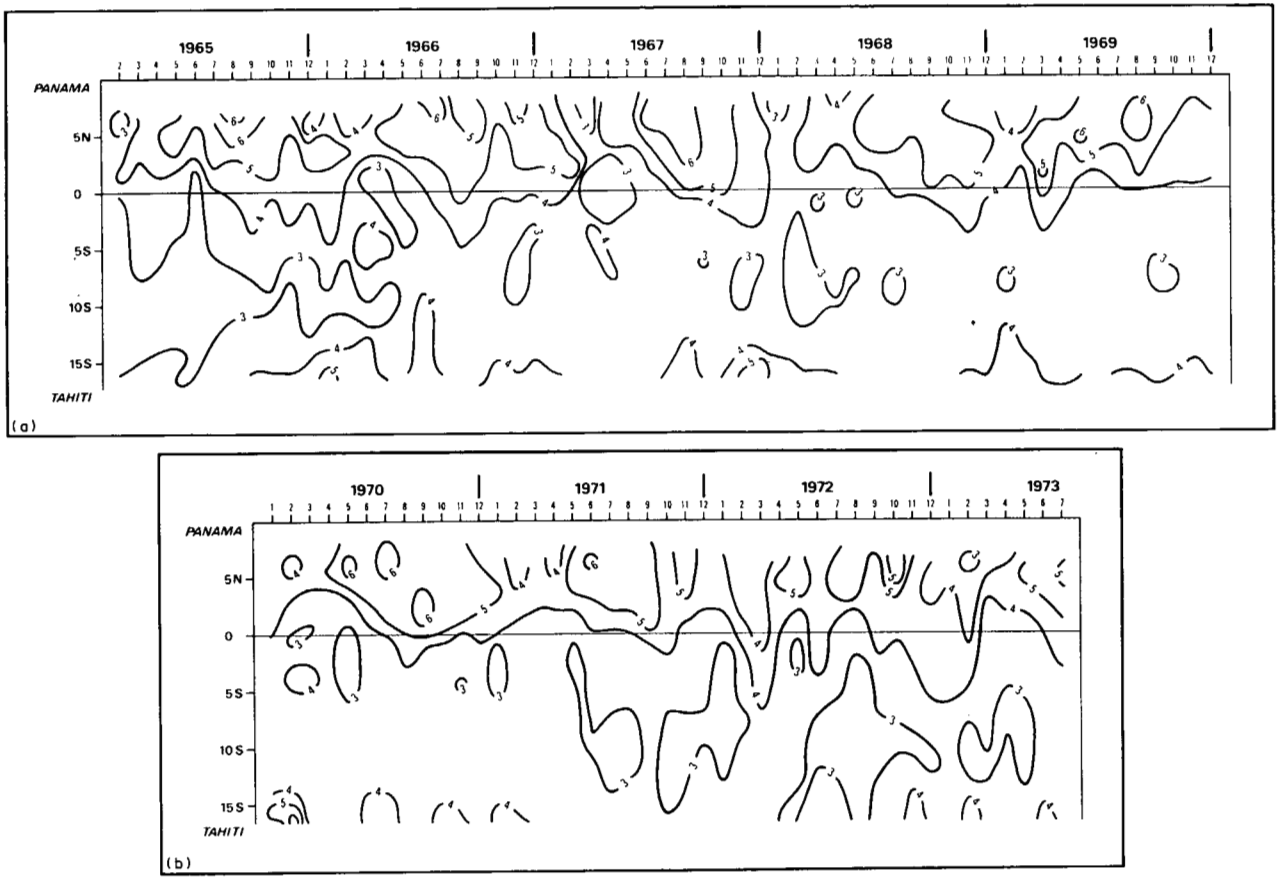

Fig. 6. Cloud cover, observed from satellites, in oktas, along the track between Tahiti and Panama, 1965–1973.

On the other hand, there is a question about the location of the convergence zone of the wind between February and May. According to ATKINSON and SADLER (1970) the zone at this time is east of 95°W, i.e., east of the ship track. According to WYRTKI and MEYERS (1975), the feature is at its southernmost location but always in the northern hemisphere (Fig. 4). In the reverse, during this period, a cloud zone exists between 1 and 5°S (Fig. 5). Consequently one may hypothesize two convergence zones, one in each hemisphere, the southern one associated with extensive cloud cover. The cloudiness would cause heavy precipitation south of the equator; at Puerto Baquerizo (Galapagos Islands, 00°54'S, 89°37'W), the maximum rainfall (Fig. 7) occurs in February and March. TAYLOR (1973), considering rainfall data, and WYRTKI and MEYERS (1976) also suggest this relationship.

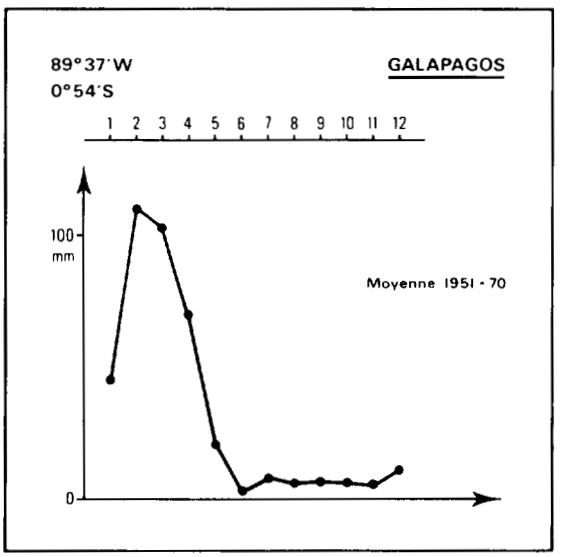

Fig. 7. Rainfall, in millimeters, at Puerto Baquerizo (Galapagos Islands, 00°54'S, 89°37'W).

2. *Year-to-year variations.* The 1955 to 1978 series of surface temperatures (Fig. 1) shows not only seasonal variations but also year-to-year variations of the equatorial upwelling intensity. Upwelling intensity may be characterized on the space–time diagram by the recorded temperature, by the duration, and by the latitude extremes. The parameters can be measured by estimating the area enclosed by an isotherm.

In Fig. 1, the area with temperatures less than 24°C is maximal in 1955, 1967, 1970, 1973, 1975 (Fig. 8), years when the equatorial upwelling was strong; the Eastropac expeditions emphasized the 1967 maximum. The area is minimal in 1957, 1963, 1965, 1969, 1972, 1976, and decreases to zero in 1957, 1965, and 1972. The last three years were marked by major El Niño phenomena, whereas in 1963, 1969, and 1976, weak upwelling and minor El Niño events were observed.

As with the surface temperatures, the area inside lines of equal cloud cover appears to be a significant parameter. In Fig. 4, the area with cloud covers of more than 7 oktas (Fig. 8) north of the equator is also minimal in 1957, 1963, 1965, 1969, and 1972, years

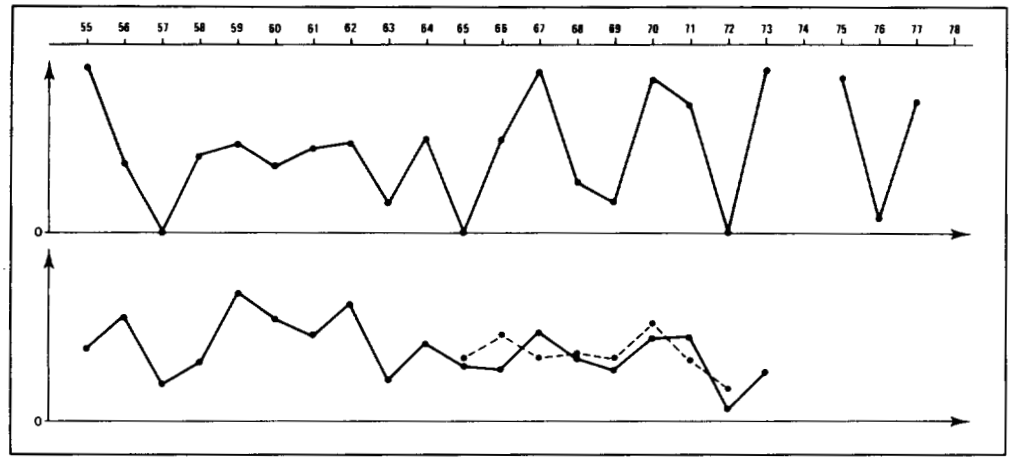

Fig. 8. In the upper part, area included within the 24°C isotherm. In the lower part, the points mark the surface bounding the cloudiness of more than 7 oktas observed from ships. The stars mark the surface bounding the cloudiness of more than 5 oktas observed from satellites. In ordinate any scale may be used.

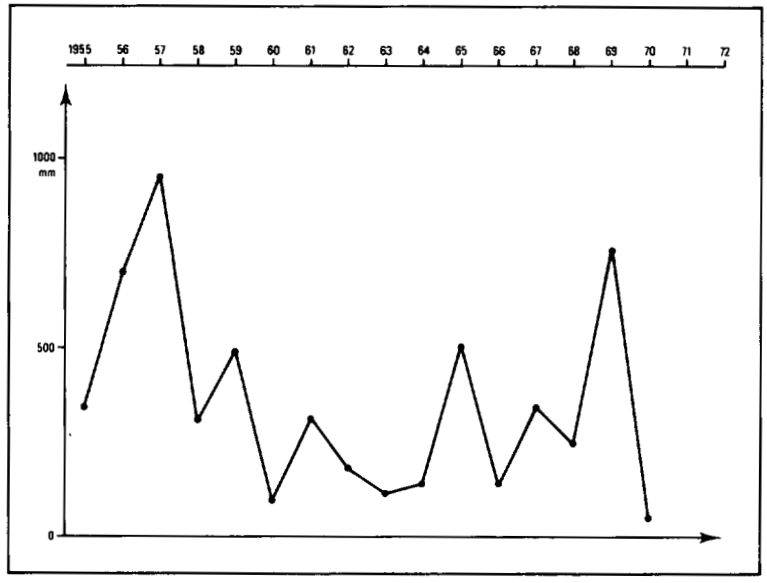

Fig. 9. Annual rainfall in millimeters at Puerto Baquerizo, 1955–1970.

characterized by El Niño phenomena. The 1965–1973 series of satellite observations shows the same trend.

In the case of El Niño, the cooling induced by equatorial upwelling is minimum and, on the equator, the sea surface temperature is maximal and cloud cover in the northern hemisphere is also minimal (Fig. 8). This feature confirms that high sea surface temperature is related on the equator to low cloud cover, in contradiction to BJERKNES (1966, 1969).

However, during El Niño events, mainly from March to May, cloud zones are evident south of the equator (Figs 4, 6) as in 1957, 1965, and 1972. This feature would support the hypothesis of the simultaneous presence of northern and southern convergence zones, the latter bringing rainfall; at Puerto Baquerizo precipitations were maximal in 1957, 1965, and 1969 (Fig. 9).

Surface salinity in the eastern Pacific

Since 1974 surface salinity has been observed by merchant ships between Tahiti and Panama. The series is 4 yr long with a good density of measurements (average of 3 voyages per month). The data are shown in a space–time diagram (Fig. 10) including the whole series and as the monthly average of all data (Fig. 11).

Surface conditions in the northern and southern hemispheres are very different. North of the equator, the surface salinity is usually less than 35.0‰ and even less than 34.0‰ north of 3°N. South of the equator, the surface salinity is usually more than 35.0‰ and even more than 36.0‰ south of 13°S.

Seasonal variations are also evident. Along the track from January to June, i.e., times of no equatorial upwelling, the salinity is minimal. From July to December, i.e., during equatorial upwelling, the salinity is maximal. Without equatorial upwelling, low-salinity water appears south of the equator. Along the track of the ships, this water is on the equator in March, at 5°S in April, 7°S in June, and at 10°S in July. It is associated in the southern hemisphere with a cloud cover of more than 4 oktas. Although advection of northern water across the equator is possible, the feature might indicate that the low-salinity water is induced by rainfall. During equatorial upwelling the low-salinity water remains north of the equator because of the equatorial salinity front. According to the Eastropac Atlases the front is due to the contact of low-salinity water with high salinity upwelled water. Thus, the front is associated with the equatorial upwelling and is at its north side. South of the equator, the salinity is more than 35.0‰.

The year-to-year variability of the surface salinity is small; 1976, characterized by a weak El Niño, does not look very different from the other years. Indeed, the ships cross the equator at 100°W, west of the Galapagos Islands, whereas El Niño phenomena usually occur between the islands and the South American coast.

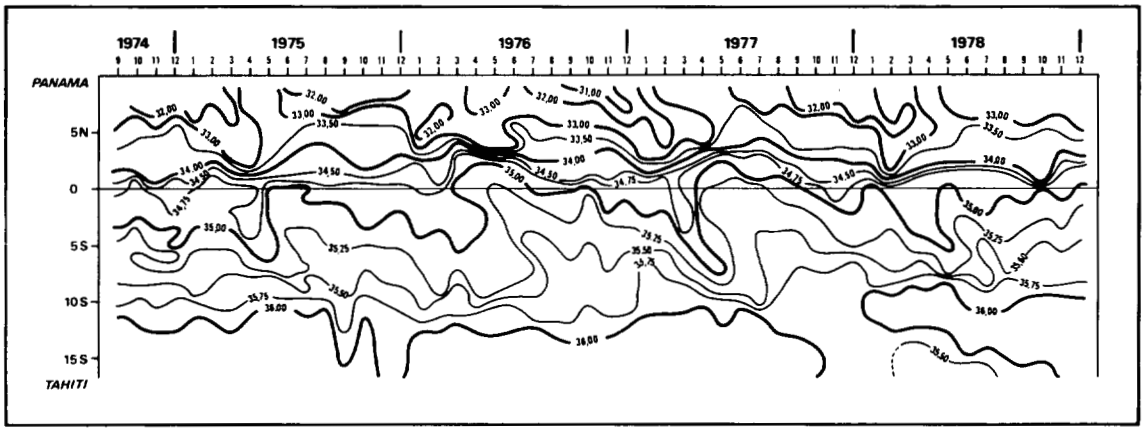

Fig. 10. Surface salinity (‰) along the track between Tahiti and Panama, 1974–1978.

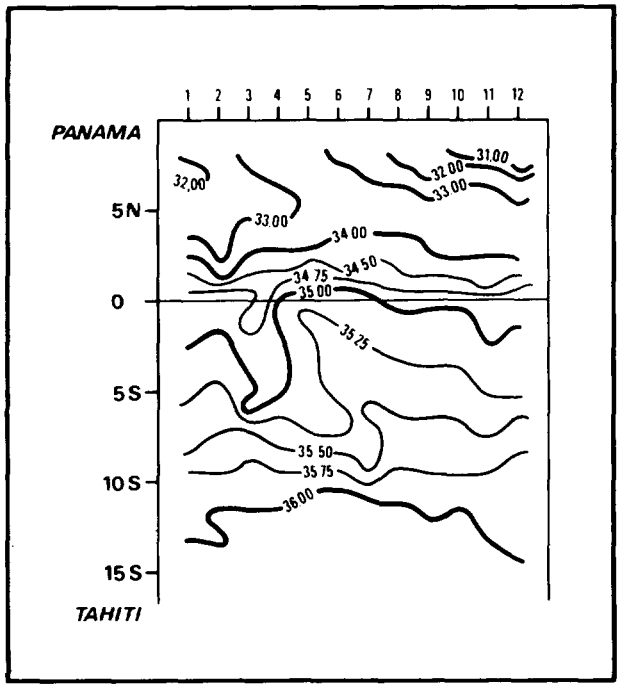

Fig. 11. Mean surface salinity (‰) along the track between Tahiti and Panama.

Surface salinity during El Niño

The El Niño phenomenon has been studied in detail; WOOSTER and GUILLEN (1974) described the 1972 El Niño, with main consideration of the surface temperature. WYRTKI, STROUP, PATZERT, WILLIAMS and QUINN (1976) observed in 1975 the surface temperature and salinity spreading of a short-lived El Niño. QUINN (1977) and MILLER (1977) made meteorological and fisheries statements about the 1976 El Niño.

From 1970 to 1977 two El Niño events with economic consequences have occurred, a drastic one in 1972 and a weaker one in 1976. Both times it was possible to draw up surface salinity charts for the concerned area (10°N–10°S, 75°W–105°W) before (November–December), during (February–March), and after (April–May) the El Niño. The wind data were obtained from ship observations or from the *Tropical Strip Surface Charts* (National Climatic Center, Asheville, N.C., U.S.A.).

Figure 12 shows the surface salinities observed during the latter part of 1971 (mainly December) and at the end of 1975 (October–November), just before the El Niño event. In 1971 and in 1975 the wind fields were similar: the intertropical convergence zone was at 5°N, south of its usual position (10°N) (ATKINSON and SADLER, 1970). South of the intertropical convergence zone, east of 90°W, the southeasterly winds were deflected to the southwest. The equatorial salinity front separated southern high-salinity waters from the northern low-salinity ones. In 1971 and 1975, the 35.0‰ isohaline lay at 5°S and the 34.0‰ isohaline at the equator. The water with salinity less than 33.5‰ was east of 95°W.

Figure 13 shows the surface salinity observed in February–March 1972 and in February–March 1976, El Niño years. In both cases the wind field was similar but in 1972 the

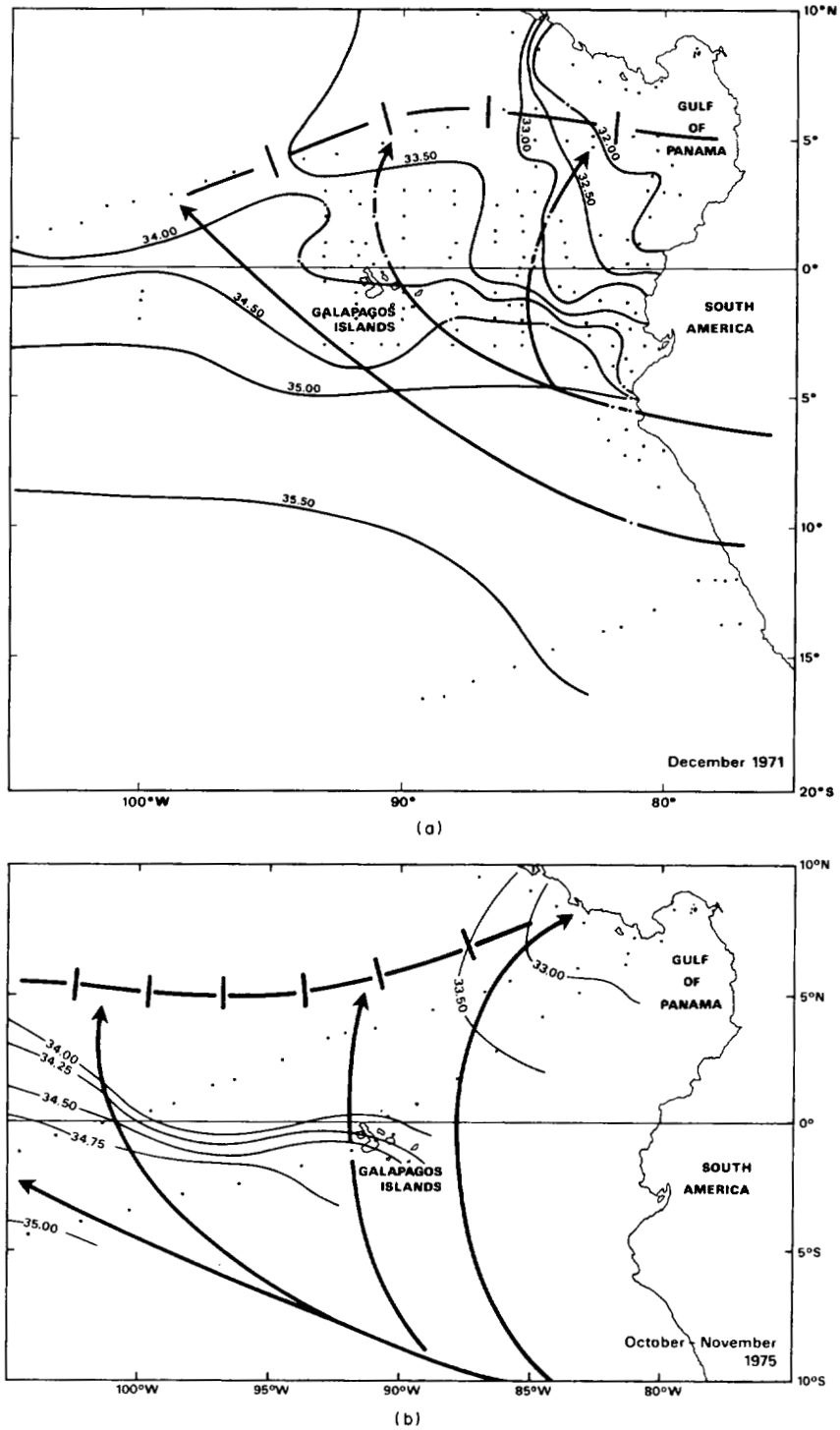

Fig. 12. Surface salinity (‰) in December 1971 and in October–November 1975 in the eastern equatorial Pacific.

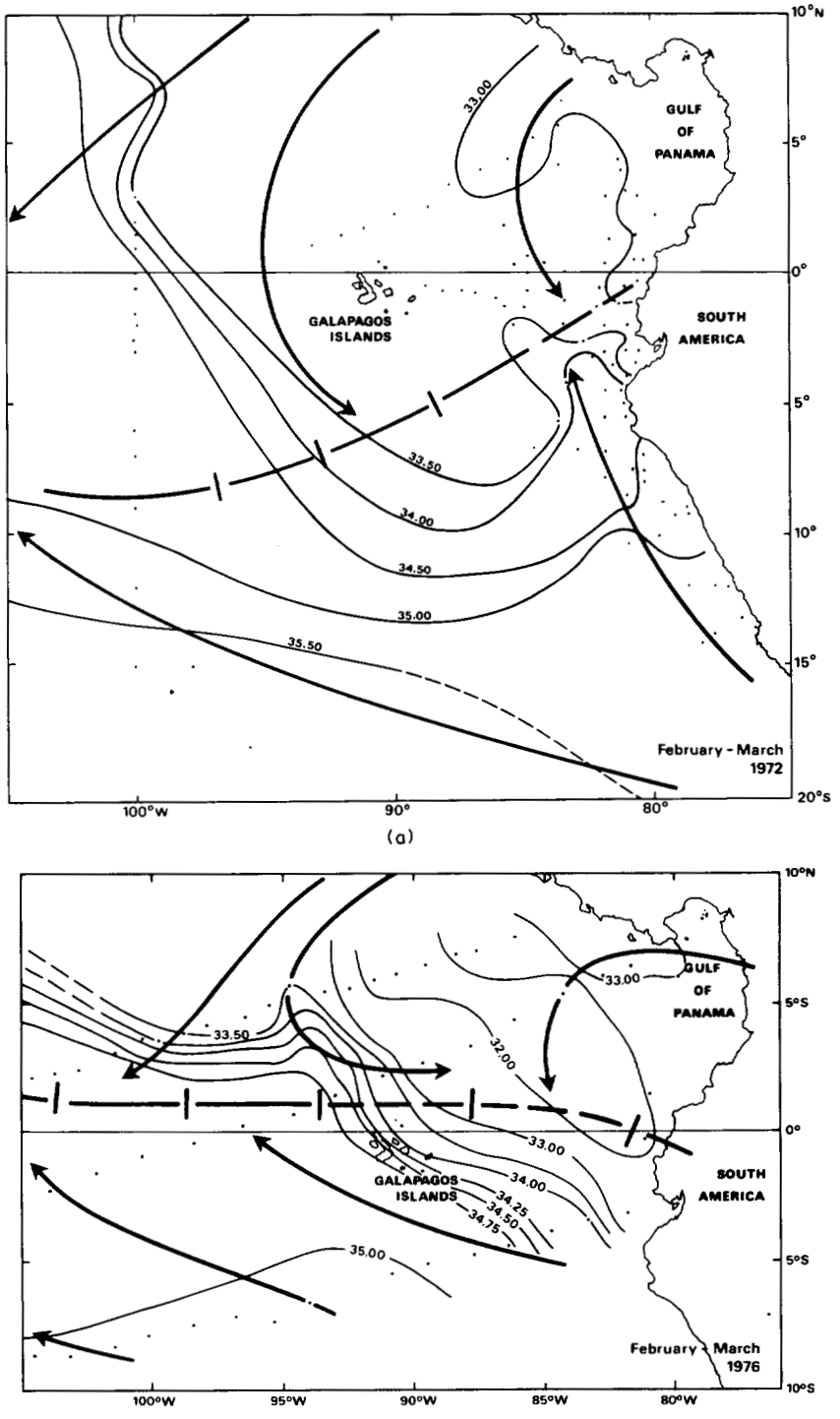

Fig. 13. Surface salinity (‰) in February–March 1972 and in February–March 1976 in the eastern equatorial Pacific.

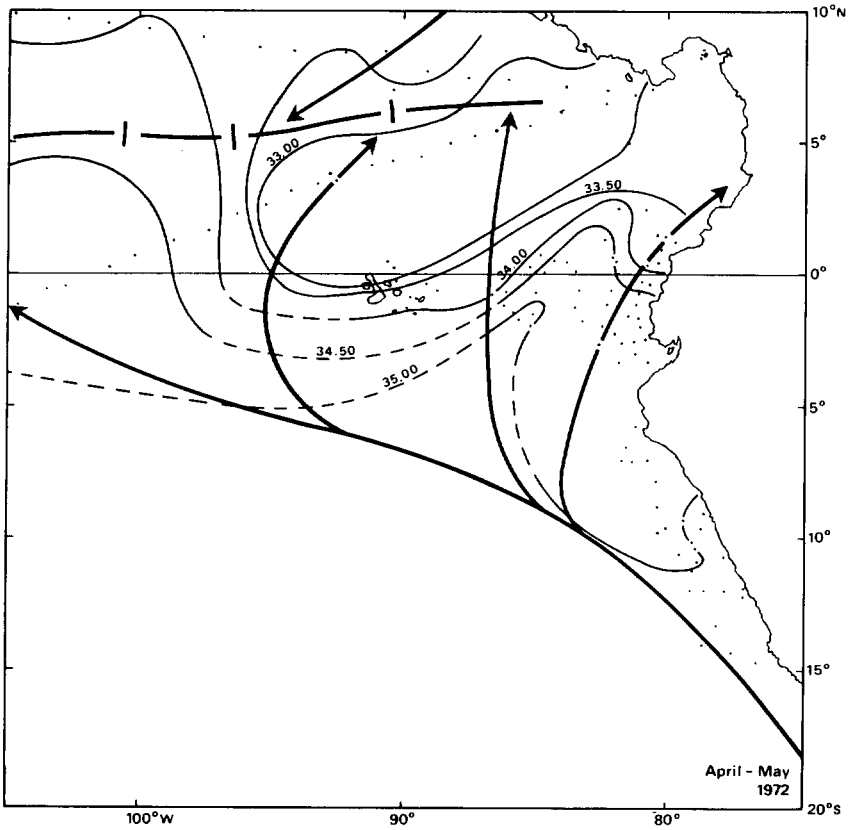

(a)

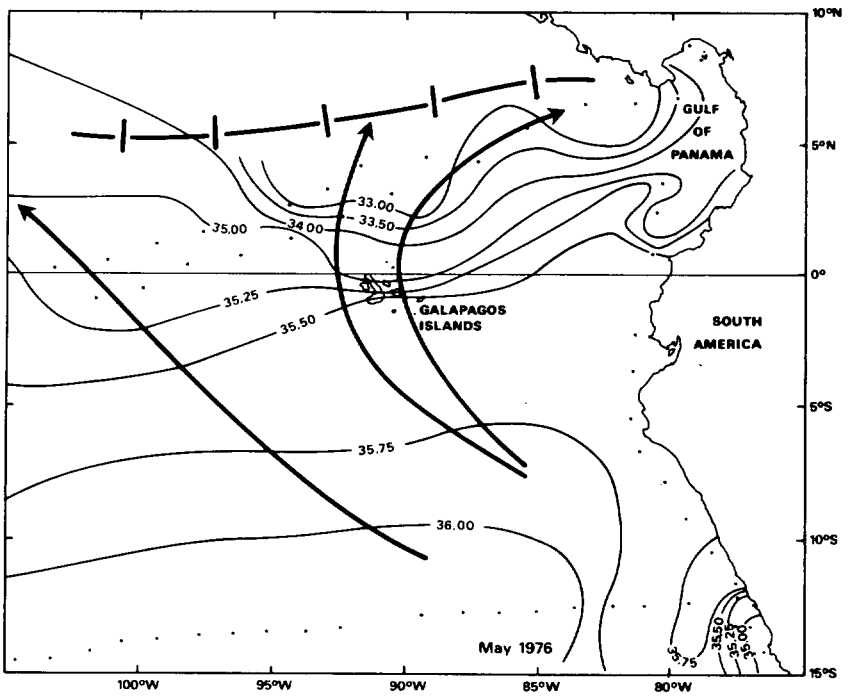

(b)

Fig. 14. Surface salinity (‰) in April–May 1972 and in May 1976 in the eastern equatorial Pacific.

intertropical convergence zone was between the equator and 10°S and in 1976 at 1°N; the presence of a convergence zone at 10°S in 1972 is consistent with the hypothesis that this is a double feature. South of the convergence zone, the winds were from the southeast. North of the convergence zone, northeasterly winds prevailed but east of 95°W they were deflected to the northwest. The west-component wind was not compatible with equatorial upwelling. The absence of upwelling allowed the low-salinity water to spread into the southern hemisphere and consequently the equatorial front disappeared. In 1972 the 33.0‰ isohaline reached nearly to 8°S; in 1975 it reached nearly to 5°S, but the low-salinity water spread into a smaller area than in 1972.

Figure 14 shows the surface salinity observed in April–May 1972 and in May 1976, after the El Niño event. The same kind of wind fields occurred: the intertropical convergence zone lay at 7°N, a position close to the usual, 10°N. South of the convergence zone, a southeast wind prevailed, deflected to the southwest east of 95°W and north of the equator. West of 95°W the wind was favorable to equatorial upwelling; consequently, the equatorial front occurred there. A tongue of high-salinity water, due to coastal upwelling induced by the southeast wind, crossed the equator near 80°W. The low-salinity water ($S < 33.5‰$) was north of the equator, mainly east of 95°W.

Influence of the position of the intertropical convergence zone in the eastern equatorial Pacific

In the case of the 1972 and 1976 El Niño events the spreading of the low-salinity water seems to be related to the position of the intertropical convergence zone: in November–December (Fig. 12), before the El Niño event, the intertropical convergence lay at 5°N and the core of the low-salinity water was at this latitude. In February–March (Fig. 13), during the El Niño event, the intertropical convergence zone lay close to the equator or just south of it and the low-salinity water spread across the equator and into the southern hemisphere. In April–May (Fig. 14), after the El Niño event, the intertropical convergence zone again lay in the northern hemisphere at 7°N and the low-salinity water again withdrew into the northern hemisphere.

Before and after El Niño events the convergence zone is between 5° and 10°N and the wind field associated with it has two consequences: along the South American coast a southeast wind parallel to the shore induces coastal upwelling; along the equator, west of 90°W, the southeast wind induces equatorial upwelling.

During El Niño events, the convergence zone is south of its usual location. According to ATKINSON and SADLER (1970) in February it usually lies at 10°N. During Eastropac cruises, its position was around 5°N. Figure 15 shows the position of the convergence zone at 90°W from January to March in 1972 and 1976 according to the *Tropical Strip Surface Charts*. Its exceptional presence south of the equator is evident at 2°S in February 1972, at 8°S in March 1972, at 3°S in February 1976, and at 5°S in March 1976; in many cases the southern convergence zone coexists with a northern one. PATZERT (1978) showed the same feature in February–March 1975. The anomalous position of the convergence zone is associated with an anomalous wind field. South of 5°S, southeast winds prevail along the coast and induce the usual coastal upwelling. West of 100°W, northeast or southeast winds blow along the equator and induce the usual equatorial upwelling. But east of 100°W northwest winds prevail along the equator and equatorial upwelling ceases. The low-salinity water pushed by northwest winds then crosses the equator into the southern hemisphere.

The direct influence of the intertropical convergence zone on the formation of low-salinity water masses by precipitation is an important consideration. The convergence zone

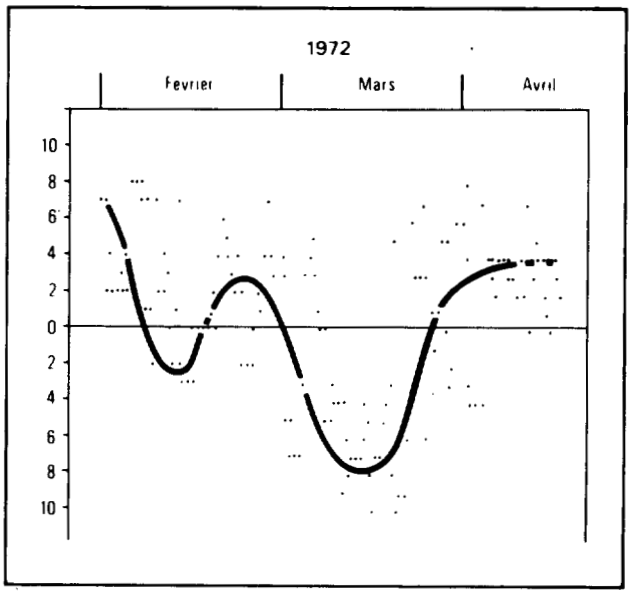

(a)

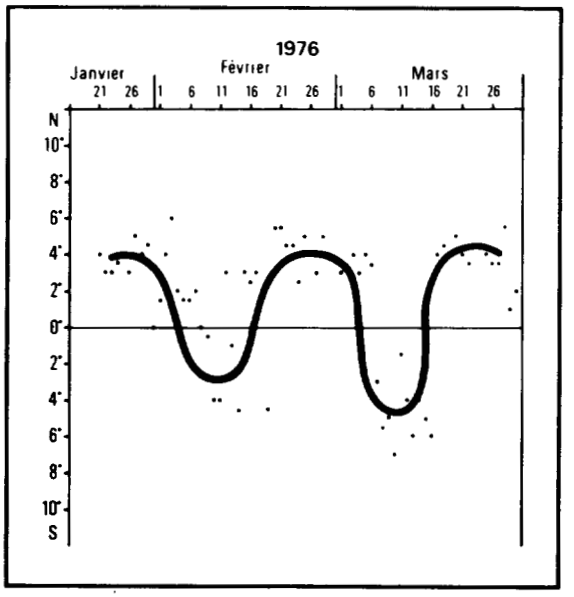

(b)

Fig. 15. Position of the intertropical convergence zone of the winds in early 1972 and 1976 along 90°W.

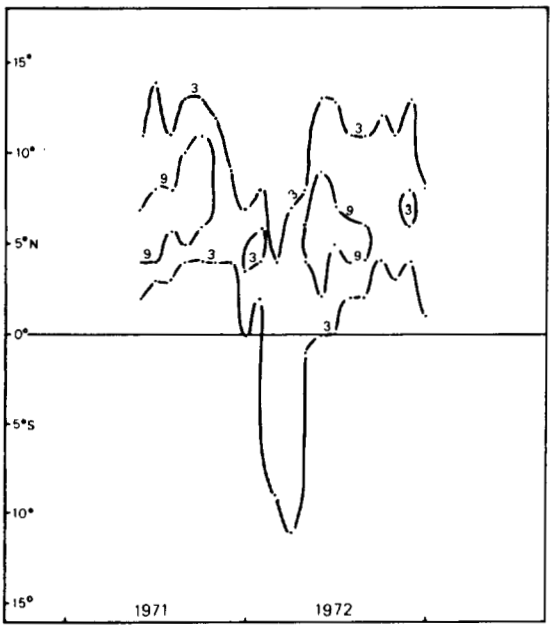

Fig. 16. 1971–1972 monthly frequencies of highly reflective clouds along 90°W.

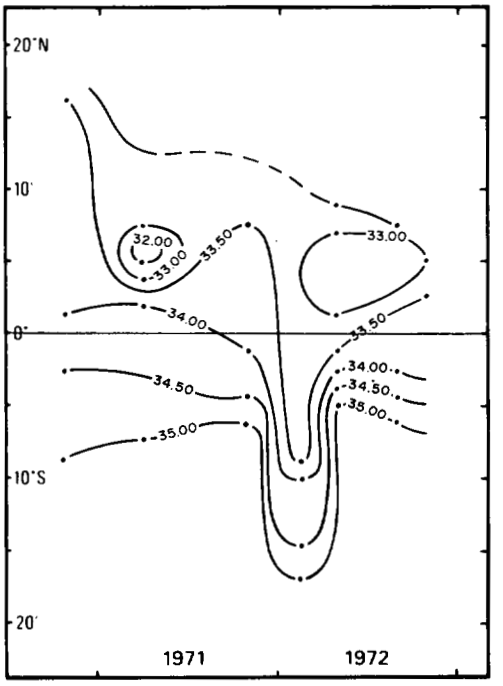

Fig. 17. 1971–1972 surface salinity (‰) along 90°W.

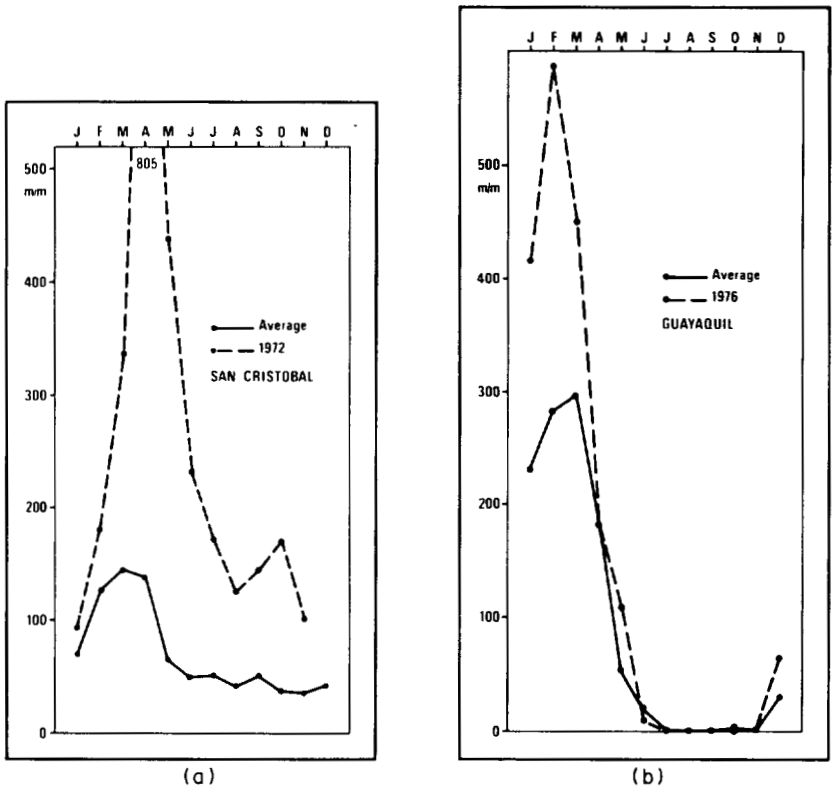

Fig. 18. Rainfall at San Cristobal (Galapagos Islands, 00°54'S, 89°37'W) and at Guayaquil (02°09'S, 79°53'W).

is usually marked by nebulosity and heavy precipitations. From 1971 to 1974 charts of the frequency of highly reflective cloud cover, as observed by satellite over the Pacific Ocean, were drawn up by KILONSKY and RAMAGE (1976). Highly reflective clouds are generally associated with precipitation and correlations have been found between their frequency and rainfall. The 1971–1972 monthly frequencies along the 90°W meridian are shown in a distance–time diagram (Fig. 16). The 1971–1972 surface salinity along the 90°W meridian (Fig. 17), extracted from the 1970–1977 quarterly charts of the eastern tropical Pacific, is also plotted on a distance–time diagram to show the variation of the surface salinity from 10°N to 20°S during 3 yr. Figures 16 and 17 are similar. The low salinities are associated with highly reflective cloud frequencies, that is to say those with a strong probability of precipitation. Low salinities and highly reflective cloud frequencies usually occur between the equator and 20°N, except in the beginning of 1972, when they occurred as far south as 10°S. During that El Niño period the 33.5‰ isohaline reached 10°S and according to KILONSKY and RAMAGE (1976) the highly reflective cloud frequencies provided 200 mm rainfall per month, thereby maintaining the low salinity of the water coming from the northern hemisphere. This feature is consistent with the rainfall observations (Fig. 18) at San Cristobal (Galapagos Islands) (00°54'S, 89°37'W) in 1972 and at Guayaquil (02°09'S, 79°53'W) in 1976. At San Cristobal between February and June 1972 precipitation was far

above average. At Guayaquil between January and April 1976, precipitation was about twice the average.

Two mechanisms may be involved in the formation of the low-salinity water during El Niño: advection of northern water and dilution by local rainfall. The influence of each of the mechanisms can be estimated: according to DONGUY and HENIN (1976), one can compare the ratio of the observed surface salinity to the mean salinity with the ratio of the simultaneously observed rainfall to the mean observed rainfall. If the ratios are the same, the salinity variation would be due completely to the rainfall; if the salinity ratio is different, another mechanism would be involved. During the 1972 El Niño the salinity ratio at 5°S is twice the rainfall one.* Consequently the salinity change would be due half to an advection across the equator of the northern low-salinity water, half to local formation from rainfall.

CONCLUSION

In the eastern equatorial Pacific Ocean, surface temperature and salinity features are usually associated with the position of the Intertropical Convergence Zone. The shifting of this zone to the south has an effect on surface conditions in two ways: it changes the wind field such that equatorial upwelling subsides and it produces low-salinity water by precipitation. The recent equipping of merchant ships with expendable bathythermographs (XBT) will improve our knowledge of these important features.

REFERENCES

ATKINSON F. D. and J. C. SADLER (1970) Mean cloudiness and gradient level wind over the tropic. Air Weather Service, United States Air Force, 15 pp., 38 charts.

BJERKNES J. (1966) A possible response of the atmospheric Hadley circulation to equatorial anomalies of ocean temperature. *Tellus*, **18**, 820–829.

BJERKNES J. (1969) Atmospheric teleconnections from the equatorial Pacific. *Monthly Weather Review*, **97**, 163–172.

* The calculation is based on the assumption that the salinity increases linearly from the surface to a depth d. The height of freshwater h that can induce the surface freshening is expressed by

$$h = \tfrac{1}{2}d\left(\frac{S_1 - S_2}{S_1}\right),$$

where S_1 is a constant salinity at the depth d, S_2 is either the observed surface salinity S_{obs} or the mean surface salinity S_{mean}. In the first case

$$h_{obs} = \tfrac{1}{2}d\,\frac{S_1 - S_{obs}}{S_1}.$$

In the second case

$$h_{mean} = \tfrac{1}{2}d\,\frac{S_1 - S_{mean}}{S_1}.$$

The ratio

$$R_s = \frac{h_{obs}}{h_{mean}} = \frac{S_1 - S_{obs}}{S_1 - S_{mean}}$$

can be compared with the ratio

$$R_p = \frac{\text{observed precipitation}}{\text{mean precipitation}}.$$

In the case of the 1972 El Niño, $S_1 = 35.2‰$ (PATZERT, 1978), $S_{obs} = 33.5‰$, $S_{mean} = 35.0‰$ and consequently $R_s = 8.5$. During the time, the observed precipitation was 200 mm instead of a mean of 50 mm (TAYLOR, 1973) and consequently $R_p = 4$.

CROMWELL T. (1953) Circulation in a meridional plane in the Central Equatorial Pacific. *Journal of Marine Research*, **12**, 196–213.

DONGUY J. R. and C. HENIN (1976) Relations entre les précipitations et la salinité de surface dans l'Océan Pacifique tropical sud-ouest basées sur un échantillonnage de surface de 1956 à 1973. *Annales Hydrographiques*, 5e série, **4**, 53–59.

HIRES R. I. and R. B. MONTGOMERY (1972) Navifacial temperature and salinity along the track from Samoa to Hawaii, 1957–1965. *Journal of Marine Research*, **30**, 177–200.

KILONSKY B. J. and C. S. RAMAGE (1976) A technique for estimating tropical open ocean rainfall from satellite observations. *Journal of Applied Meteorology*, **15**, 972–975.

LOVE C. M. (1972) *Eastropac Atlas*, 1, U.S. Department of Commerce.

LOVE C. M. (1975) *Eastropac Atlas*, 9, U.S. Department of Commerce.

MILLER F. R. (1977) The El Niño of 1976–77 in the southeast Pacific. Proceeding of the 2nd Annual NOAA Climate Diagnostic Workshop. Scripps Institution of Oceanography, La Jolla California, October 18–20, 1977.

PATZERT W. (1978) El Niño watch atlas of physical, chemical and biological oceanographic and meteorological data. Scripps Institution of Oceanography, Reference Series Number 78–7, 24 pp., 322 figs.

QUINN W. H. (1977) Diagnosis of the 1976–77 El Niño. Proceeding of the 2nd Annual NOAA Climate Diagnostic Workshop. Scripps Institution of Oceanography, La Jolla, California, October 18–20, 1977.

RAMAGE C. S. (1977) Sea surface temperature and local weather. *Monthly Weather Review*, **105**, 540–544.

SADLER J., L. UDA and B. J. KILONSKY (1976) Pacific Ocean cloudiness from satellite observations. Publication UHMET 76–01, Department of Meteorology, University of Hawaii, 137 pp.

TAYLOR R. C. (1973) An atlas of Pacific islands rainfall. Data Report No. 25, HIG 73–9, University of Hawaii, 165 pp, 13 figs. (Unpublished document.)

WOOSTER W. S. and O. GUILLEN (1974) Characteristics of El Niño in 1972. *Journal of Marine Research*, **32**, 387–403.

WYRTKI K. and G. MEYERS (1975) The trade wind field over the Pacific Ocean. Part 2 Bimonthly fields of wind stress: 1950 to 1972. Publication HIG 75–2, University of Hawaii, 16 pp, 138 figs. (Unpublished document.)

WYRTKI K. and G. MEYERS (1976) The trade wind field over the Pacific Ocean. *Journal of Applied Meteorology*, **15**, 698–704.

WYRTKI K., E. STROUP, W. PATZERT, R. WILLIAMS and W. QUINN (1976) Predicting and observing El Niño. *Science* **191**, 343–346.